Supporting information: Exploring a proximity-coupled Co chain on Pb(110) as a possible Majorana platform

Michael Ruby,[†] Benjamin W. Heinrich,[*,†] Yang Peng,[†,‡] Felix von Oppen,[†,‡] and Katharina J. Franke[†]

Fachbereich Physik, Freie Universität Berlin, 14195 Berlin, Germany, and Dahlem Center for Complex Quantum Systems, Freie Universität Berlin, 14195 Berlin, Germany

E-mail: bheinrich@physik.fu-berlin.de

Phone: +49 (0)30 838 52 807

[*]To whom correspondence should be addressed

[†]Fachbereich Physik, Freie Universität Berlin, 14195 Berlin, Germany

[‡]Dahlem Center for Complex Quantum Systems, Freie Universität Berlin, 14195 Berlin, Germany

Spin-polarized measurements

As described in the main manuscript, we preformed spin-polarized measurements[1] with a cobalt-covered tungsten tip. The tip was cleaned in situ by Ne^+ ion sputtering and then coated with two to four layers of cobalt (Co) by e-beam evaporation from a rod. The out-of-plane spin sensitivity of the tip was determined by measurements on the well-established system of two monolayer-high Co islands on Cu(111)[2], which posses an out-of-plane magnetization at low temperatures. We characterized the magnetic remanence of the tip by measuring the dI/dV signal as a function of applied magnetic field. A sizable remanence is essential for measuring spin contrast at zero field. All employed tips showed remanence with a coercivity of approximately ± 50 mT [Fig. S1(c)].

Spin contrast along the chain and hysteresis of the tip magnetization

In Fig. 1 of the main text, we plot a dI/dV spectrum that shows a spin-polarized resonance which we link to a van Hove singularity of a d band of the Co chain on Pb(110). For completeness, Fig. S1(a) shows a larger set of spectra along the same chain. The spectral intensity of the d band at -170 mV decreases when approaching the chain end or the cluster. However, a spin contrast is detected all along the chain.

Figure S1(c) shows the dI/dV signal at -170 mV as a function of out-of-plane magnetic field. The data points are obtained as the spatial average of the signal intensity in dI/dV maps on the chain at the respective field. A spin contrast is observed with a hysteresis loop opening around zero field. This is due to the remanence of the tip magnetization and a coercivity of approximately ± 50 mT. The switching of the tip magnetization is in line with the pre-characterization of the tip on Co islands on Cu(111) (not shown). The magnetization of the chain could not be switched in out-of-plane fields of up to ± 3 T.

In total, we checked the spin polarization of ten chains of different length. The spectral intensity of six (four) chains was higher (lower) when probed with a $\text{tip}_\uparrow$ compared to a $\text{tip}_\downarrow$ which is in agreement with a stochastic distribution.

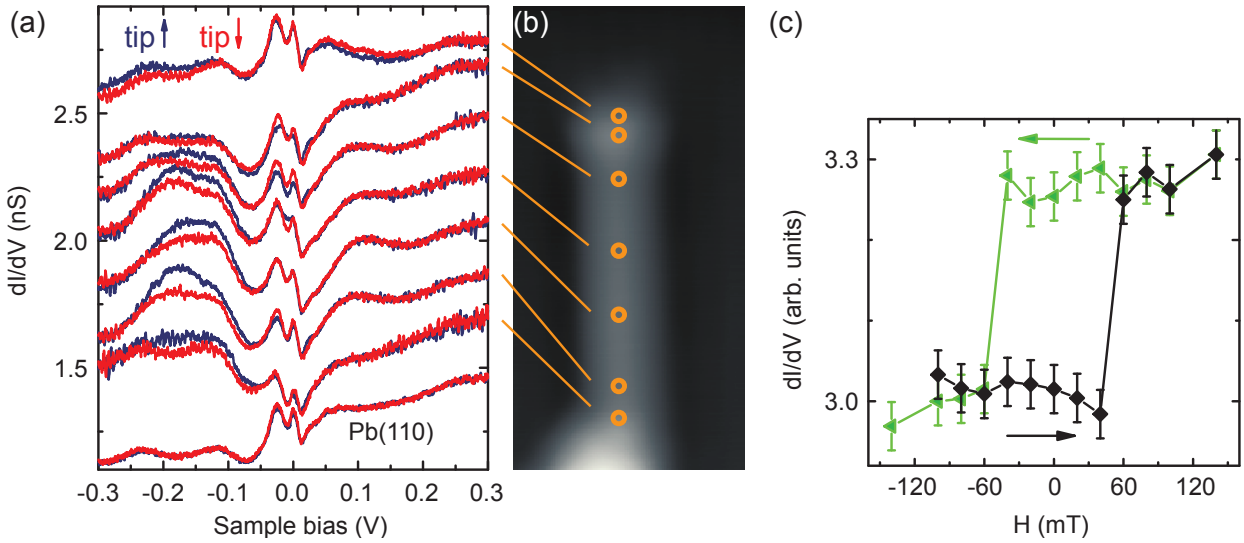

Figure S1: (a) Spin-polarized dI/dV spectra acquired at different points along the Co chain as indicated in the topography in (b) (same chain as in Fig. 1 and 2 of the main manuscript; z component of the tip magnetization indicated by arrows). Setpoint: 300 mV, 400 pA. Bias modulation: 5 $\mathrm{mV_{rms}}$. (c) dI/dV intensity at -170 mV as a function of the magnetic field strength perpendicular to the sample surface. Field sweep direction is indicated by arrows. Each data point is an average of the dI/dV intensity over the same area (1.5 $\mathrm{nm^2}$) of the chain.

Spin-polarized excitation spectra of the Yu-Shiba-Rusinov bands

In Fig. 2 of the main manuscript we showed spin-polarized dI/dV spectra of the Yu-Shiba-Rusinov (YSR) bands at the center and at the end of a Co chain. For completeness, we show a set of spectra acquired along the chain's central axis (spectra 1 to 15), and across the chain end (spectra 16 to 20) in Figs. S2(a) and (b), respectively. The signal intensities vary along the chain. However, as shown in the main text and in the next section, the difference maps are rather uniform, besides at the chain end.

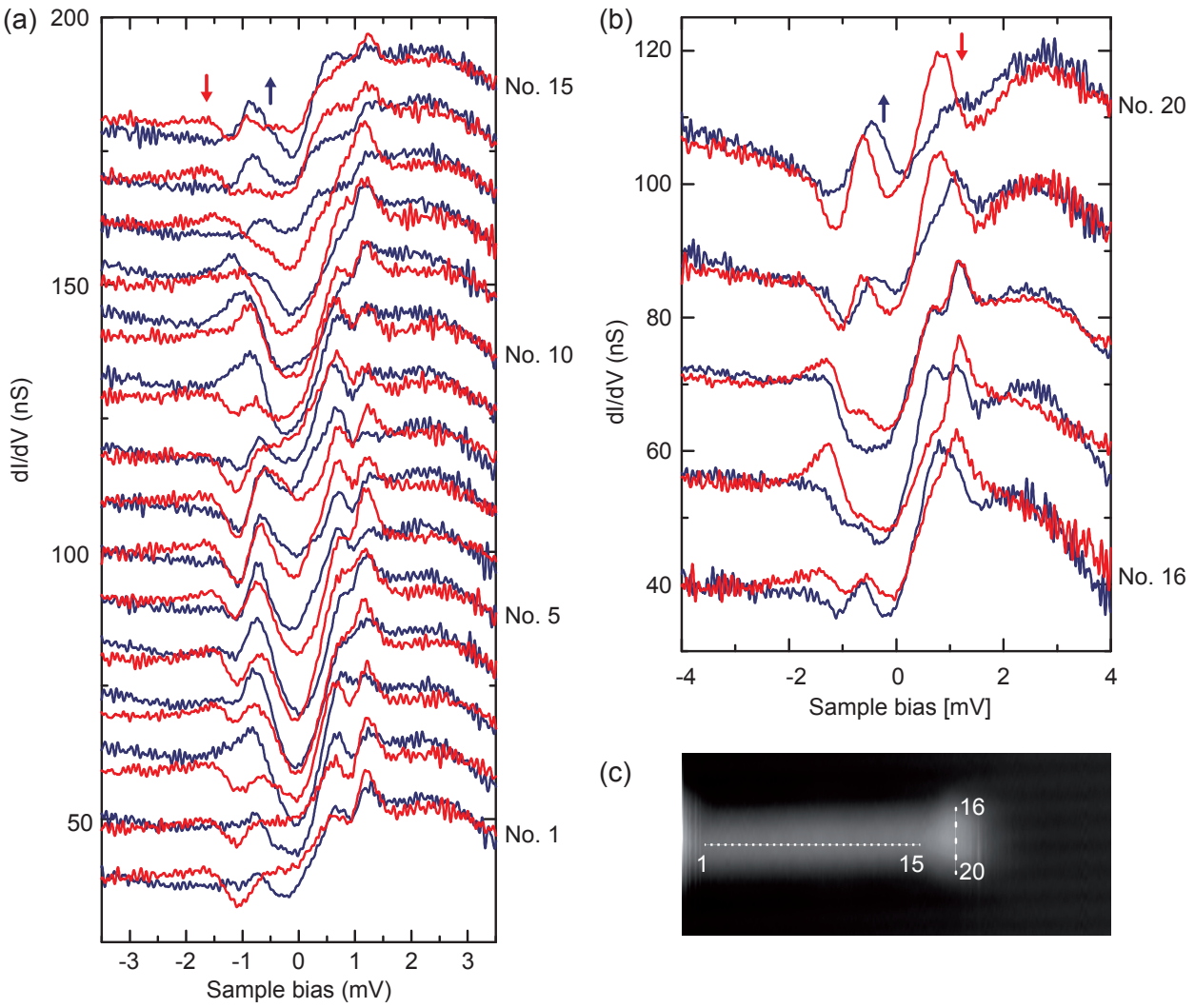

Figure S2: (a,b) Spin-polarized dI/dV spectra acquired along the body and across the chain end, as indicated in (c). Arrows indicate the orientation of the z component of the tip magnetization. Setpoint: 200 pA, 4 mV. Bias modulation: 50 μV_{rms}.

Energy-dependent spin contrast of the Yu-Shiba-Rusinov bands

The main text shows dI/dV maps of the spectral intensity along the chain at -850 μV acquired with tip$_\uparrow$ and tip$_\downarrow$, as well as a map of the signal difference in each point (spin contrast map). In Fig. S3, we show dI/dV maps at other subgap energies, as well as at 4 mV, i.e., outside the gap, for comparison. All maps reveal local variations of the spectral intensity along the chain. However, the contrast maps at ± 850 μV and ± 550 μV unveil a spin contrast along the chain, which is opposite at energies of opposite sign [Fig. S3(c)].

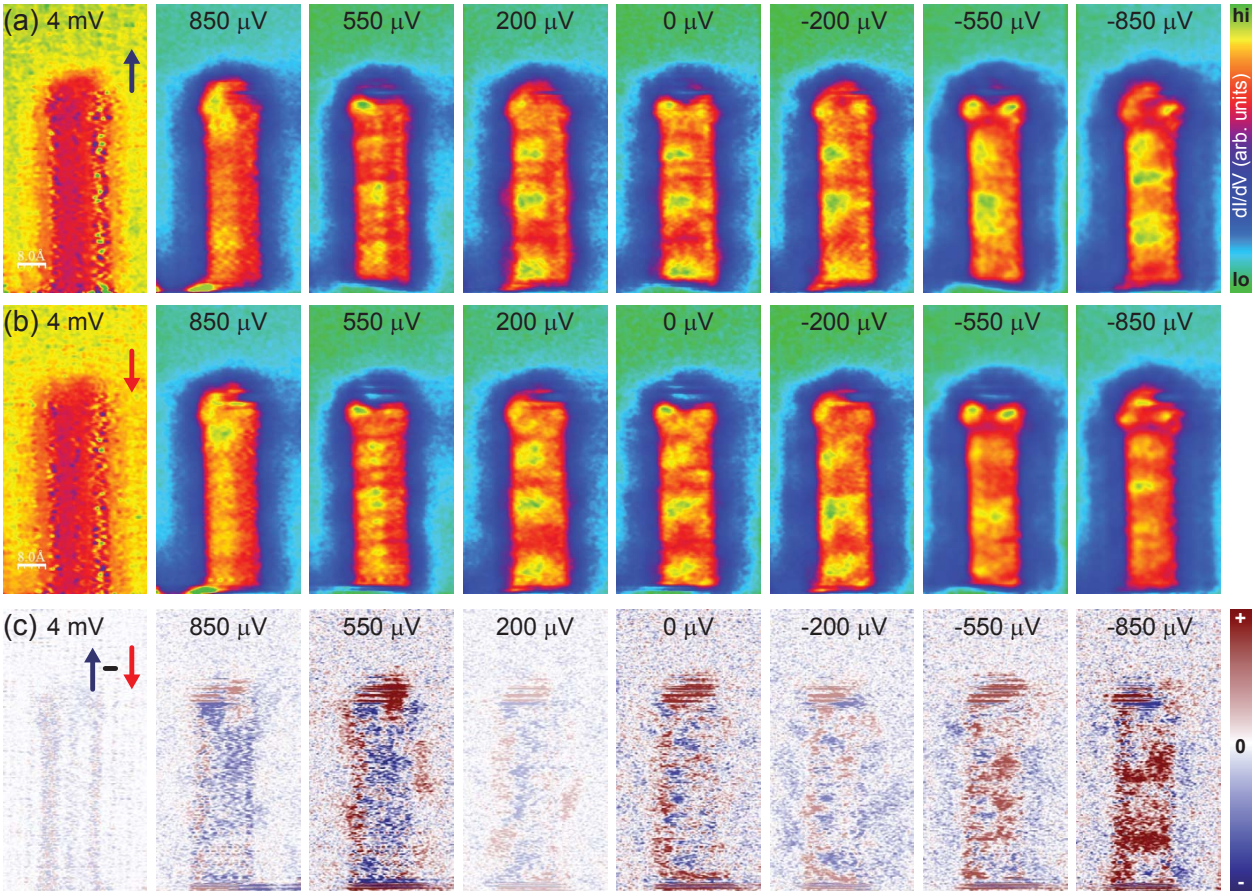

Figure S3: Spin-polarized dI/dV maps at various subgap energies. Same chain as in Fig. 1 and 2 of the main manuscript. The z component of the tip magnetization is either up (a, $\text{tip}_\uparrow$) or down (b, $\text{tip}_\downarrow$). (c) Spin contrast maps obtained by subtraction of the respective maps in (a) and (b). Setpoint: 4 mV, 200 pA. Bias modulation: 50 μV_{rms}.

Determination of the superconducting tip gap

In order to improve the energy resolution beyond the Fermi-Dirac limit we employ superconducting tips for experiments examining the subgap structure. The dI/dV spectra result form a convolution of the spectral intensity of the sample with the BCS-like density of states of the tip. One consequence of a superconducting tip with gap Δ_{tip} is a shift of a sample resonance with energy ε to a bias value of $\pm\left(\Delta_{\text{tip}}+\varepsilon\right)/e$. The exact determination of ε relies on the correct determination of Δ_{tip}.

Pb is a two-band superconductor with two gap parameters ($\Delta_1 \simeq 1.42$ meV and $\Delta_2 \simeq 1.29$ meV). They originate from two separated Fermi surfaces, and give rise to the double-

peak structure in the dI/dV spectra[3]. The tip is prepared by controlled indentation into the clean Pb surface with high voltage applied to the tip. This creates an amorphous superconducting Pb layer on the tip and yields a single gap parameter Δ_{tip}, which can be similar to or smaller than the bulk gap values, depending on the layer thickness and quality.

A spectrum acquired with such a superconducting tip on pristine Pb(110) determines the sums $\Delta_1+\Delta_{\mathrm{tip}}$ and $\Delta_2+\Delta_{\mathrm{tip}}$. Yet, an independent determination of Δ_{tip} is not straight forward. We can access the full set of independent parameters (Δ_1, Δ_2, and Δ_{tip}) using spectra with a pronounced low-energy YSR state, which gives rise to well-resolved thermal resonances (these are caused by thermally excited quasiparticles tunneling between tip and sample)[4]. To this end, we used Mn adatoms, which show such low-energy YSR resonances[4]. The YSR resonance and its thermal counterpart occur symmetric to Δ_{tip} at $\pm\left(\Delta_{\mathrm{tip}}+\varepsilon\right)$ and $\pm\left(\Delta_{\mathrm{tip}}-\varepsilon\right)$, respectively. This allows us to determine Δ_{tip} unambiguously. Then, spectra of the pristine surface acquired with the same tip show clear BCS resonances at $\Delta_{\mathrm{tip}}+\Delta_{1,2}$ and we can unambiguously determine Δ_1 and Δ_2. Because these are bulk properties of the substrate, their energy can then serve to determine Δ_{tip} for every new tip. This procedure enables a reliable determination of the energies of subgap resonances in each Co chain.

Cobalt chains without cluster termination

Self-assembled cobalt chains grow on Pb(110) at elevated temperatures along the $[1\bar{1}0]$ direction. The majority of chains ($\approx 75\,\%$) emerge from a Co cluster and possess a single free end. We focused on these chains in the main text. The length of these chains is measured between the free end and the cluster onset. Approximately $25\,\%$ of the chains are either not connected to any cluster (although one end might fall on a step edge), or they are interlinking two clusters.

In Fig. S4, we present three chains of different length not being connected to any cluster. The dI/dV spectra qualitatively exhibit the same features α, β (albeit different in details) as the spectra presented in the main text. Only the shortest chain [Fig. S4(d)] shows a less pronounced YSR resonance α at $\simeq 2.5$ meV. In all cases, the coherence peaks of the s-wave superconductor Pb are recovered within a few Ångstroms away from the chain ends. For none of the chains, we observe a localization of a zero-energy resonance at the chain ends. We rather point out that other resonance show indications of localization at the chain ends [e.g., see dI/dV maps at $\pm 1.45\,\mathrm{mV}$ and $\pm 2.31\,\mathrm{mV}$ in Fig. S4(b)].

Cobalt chains between two clusters

Figure S5 shows dI/dV spectra of three chains, which emerge between two clusters. All chains exhibit a rich subgap structure similar to the chains conntected to only one cluster or no cluster termination. Again, we observe no signatures of the localization of a state at zero energy.

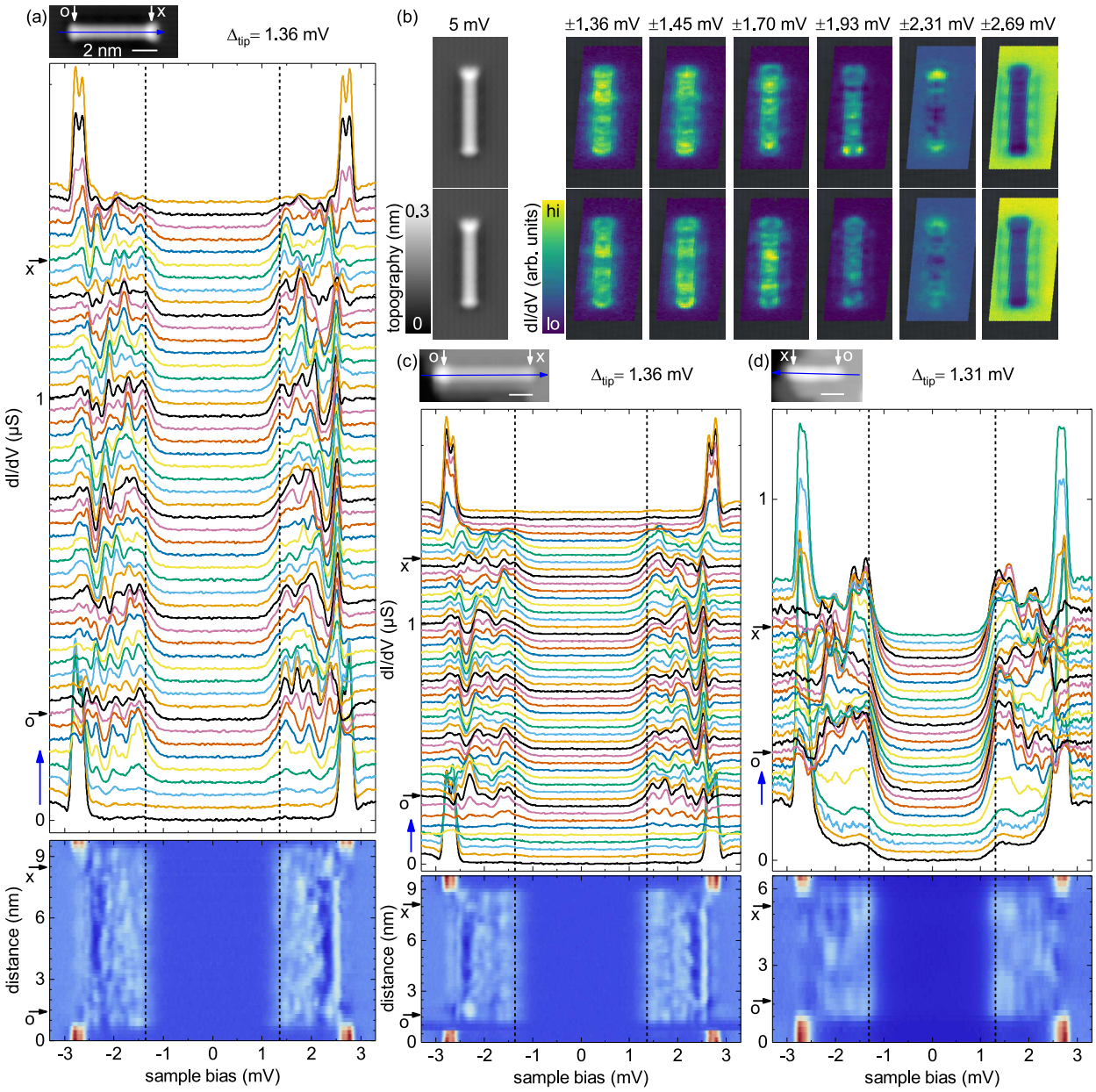

Figure S4: Three cobalt chains without a cluster at either end. The dI/dV spectra of the subgap structure in (a), (c), and (d) are acquired with a superconducting tip along the blue arrows sketched in the topography images on top of the spectra. The dashed lines mark the value of the tip gap. Zero energy excitations should appear here. A false color plot of the spectral intensity of all spectra is shown below each stacked graph. (b) shows dI/dV maps of the chain in (a) at selected energies. Feedback regulated in each point with setpoints 5 mV, 200 pA (a–c); 4 mV, 500 pA (d). Bias modulation: 15 μV_{rms}. The spectra are offset for clarity by 30 nS (a), 50 nS (c), and 23 nS (d), respectively. The lateral distance between the spectra is 200 pm (a), 196 pm (c), and 225 pm (d), respectively. The chain lengths are $\simeq$ 8.3 nm in (a) and (b), 7.5 nm in (c), and 4.1 nm in (d).

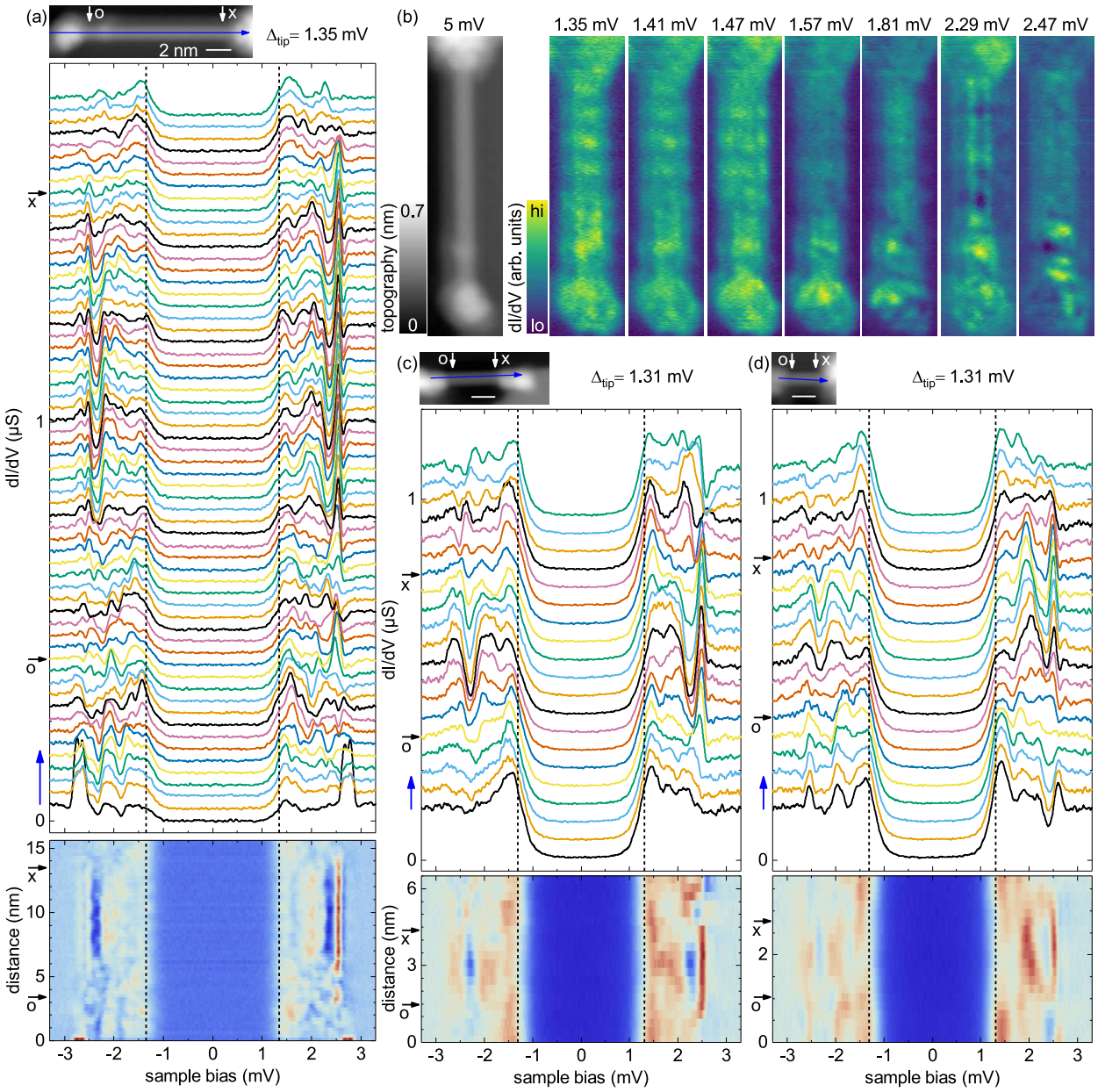

Figure S5: Three cobalt chains interlinking two clusters. The dI/dV spectra of the subgap structure in (a), (c), and (d) are acquired with a superconducting tip along the blue arrows sketched in the topography images on top of the spectra. The dashed lines mark the value of the tip gap. Zero energy excitations should appear here. A false color plot of the spectral intensity of all spectra is shown below each stacked graph. In (b), dI/dV maps at specific energies of the chain shown in (a) are plotted. The chain lengths are $\simeq$ 11.5 nm in (a) and (b), 4.1 nm in (c), and 2.8 nm in (d). The setpoint is 5 mV, 200 pA (a,b) and 4 mV, 500 pA (c,d). The spectra are offset for clarity by 30 nS (a), and 50 nS (c,d). The lateral distance between the spectra is 265 pm (a), 343 pm (c), and 200 pm (d), respectively. The bias modulation is 15 μV_{rms} for spectra (a,c,d), and 25 μV_{rms} for the dI/dV-maps (b).

Additional data on the Co chains presented in the main manuscript

In Fig. 3 of the main text, we presented dI/dV data on a chain of 10.3 nm length. For completeness, here we show additional data on the same chain. Figure S7 presents the full set of dI/dV spectra recorded along the central axis of the chain.

To image the possible localization of Majorana end states, we recorded dI/dV maps (Fig. S6) with a superconducting tip with $\pm\Delta_{\mathrm{tip}} \simeq \pm 1.35$ mV. The dI/dV maps at different subgap energies show variations in the intensity along the chain. We observe an increased intensity at the chain end for low-lying YSR states at ± 1.59 and ± 1.50 mV. The tail of these resonances spreads down to zero energy and is likely at the origin of the faint contrast increase at the chain end in the maps at ± 1.36 mV (equal to $\pm\Delta_{\mathrm{tip}}$ within the energy resolution).

In Fig. 4 of the main text, we show selected dI/dV spectra of four different Co chains on Pb(110). In Fig. S8, Fig. S9 and Fig. S10, we present the full sets of dI/dV spectra recorded along the central axis of the chains in Fig. 4(a), (b), and (c), respectively. All characteristics described in the main text are observed in these chains.

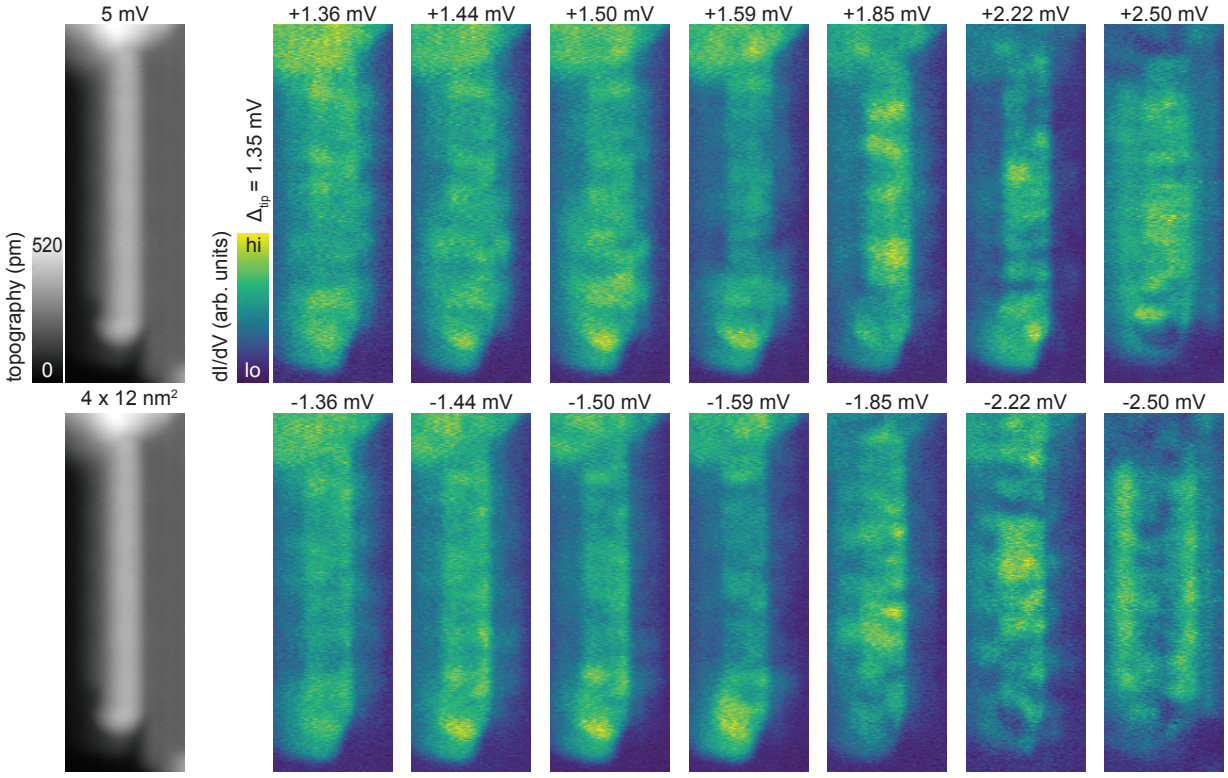

Figure S6: dI/dV maps of the Co chain on Pb(110) shown in Fig. 3 of the main text. The chain length is $\simeq$ 10.3 nm. The maps were recorded with a superconducting tip with $\Delta_{\mathrm{tip}} = 1.35$ meV. Note, that the energy resolution is $\simeq 60$ μeV. Setpoint: 5 mV, 200 pA. Bias modulation: 25 $\mu\mathrm{V}_{\mathrm{rms}}$.

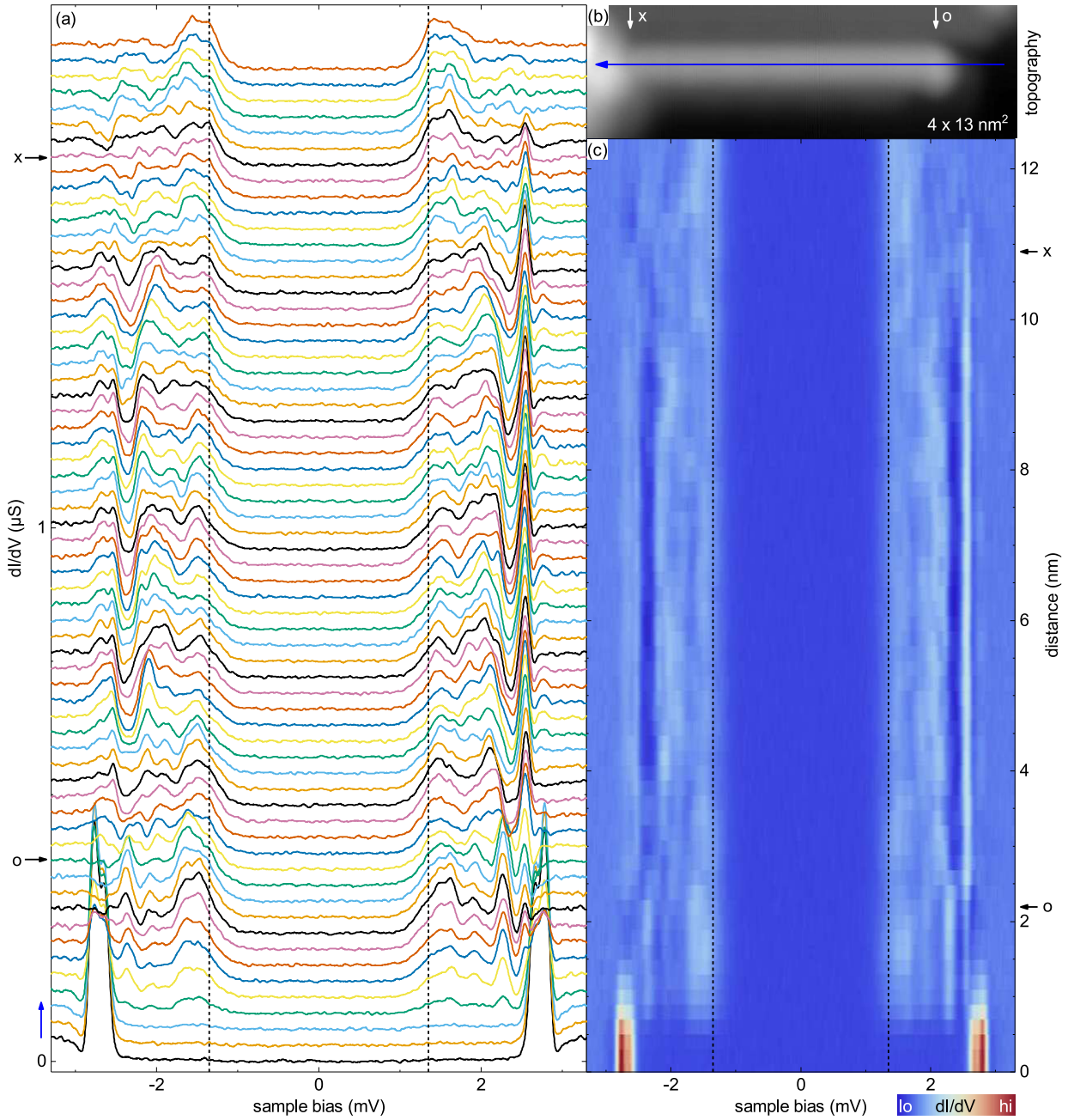

Figure S7: (a) Full set of dI/dV spectra recorded at the Co chain on Pb(110) shown in (b) along the blue arrow. The chain is the same as the one in Fig. 3 of the main text. The chain length is $\simeq$ 10.3 nm. The spectra are offset for clarity by 30 nS. The lateral distance between the spectra is 200 pm. Tip gap: 1.35 meV. Setpoint: 5 mV, 200 pA. A false color plot of the spectra is shown in (c).

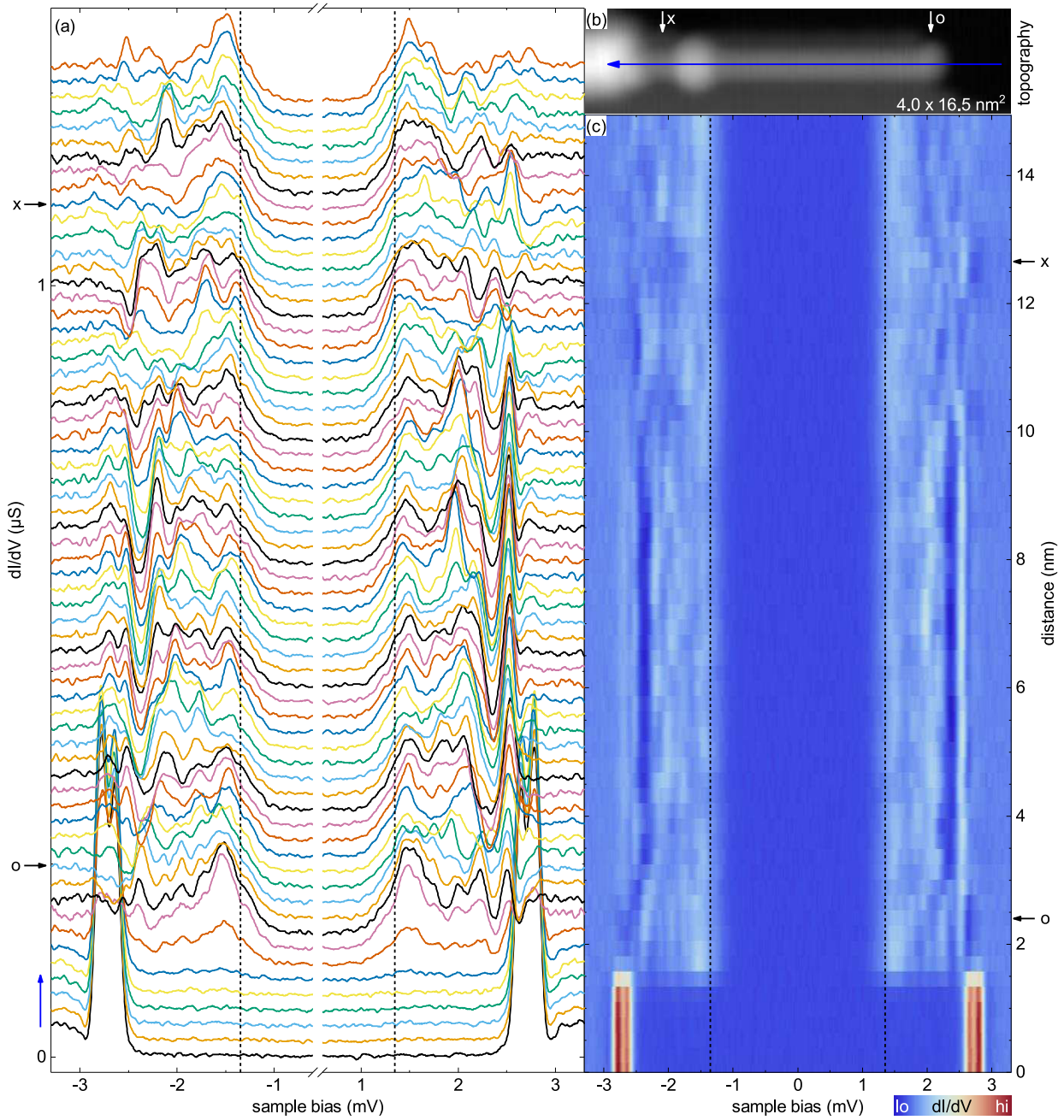

Figure S8: (a) Set of dI/dV spectra recorded at the Co chain on Pb(110) shown in (b) along the blue arrow. The chain is the same as the one in Fig. 4(a) of the main text. The chain length is $\simeq$ 11.7 nm. The spectra are offset for clarity by 20 nS. The lateral distance between the spectra is 241 pm. Tip gap: 1.35 meV. Setpoint: 5 mV, 200 pA. A false color plot of the spectral intensity of all spectra with respect to the lateral distance is shown in (c).

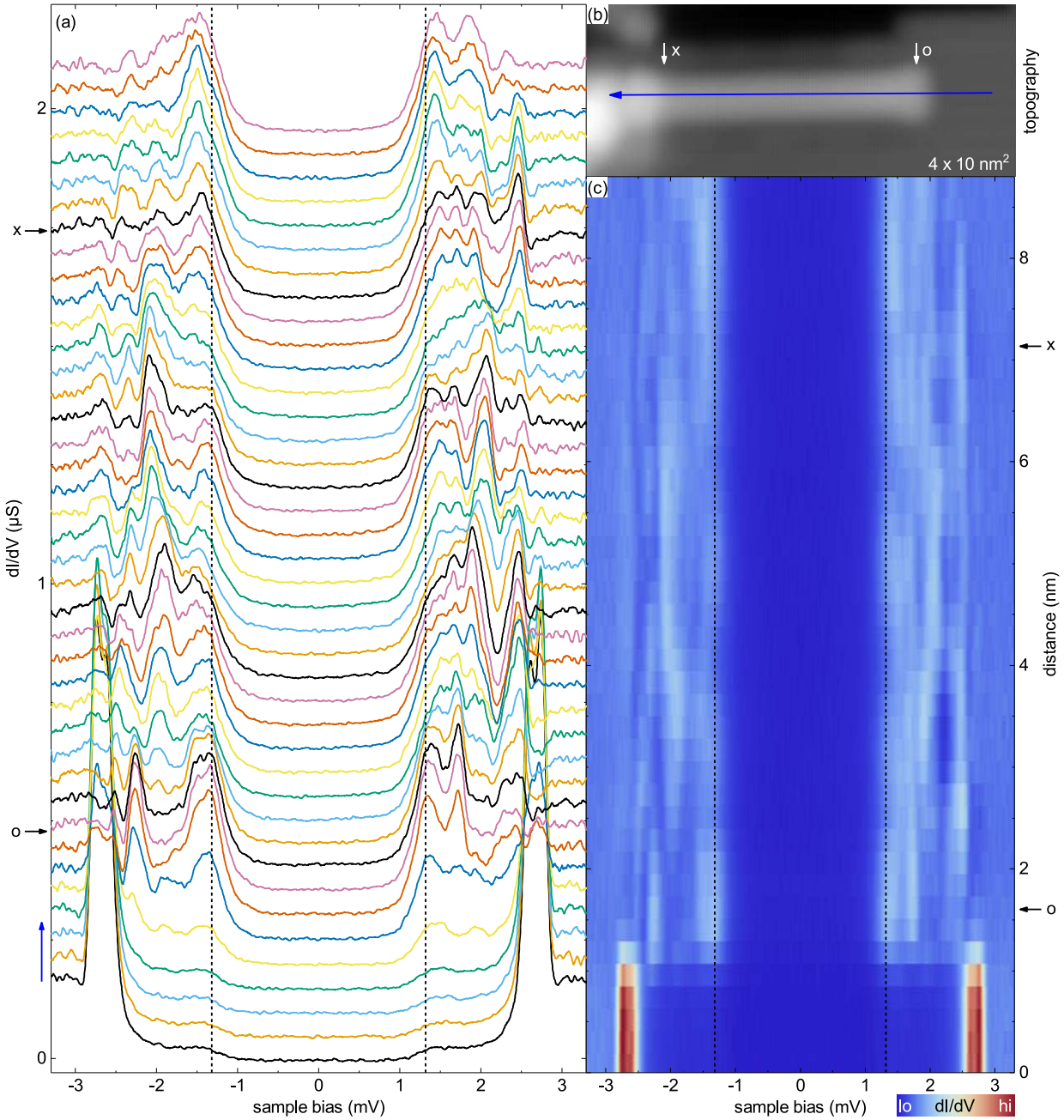

Figure S9: (a) Set of dI/dV spectra recorded at the Co chain on Pb(110) shown in (b) along the blue arrow. The chain is the same as the one in Fig. 4(b) of the main text. The chain length is $\simeq$ 6.2 nm. The spectra are offset for clarity by 50 nS. The lateral distance between the spectra is 225 pm. Tip gap: 1.32 meV. Setpoint: 4 mV, 500 pA. A false color plot of the spectral intensity of all spectra with respect to the lateral distance is shown in (c).

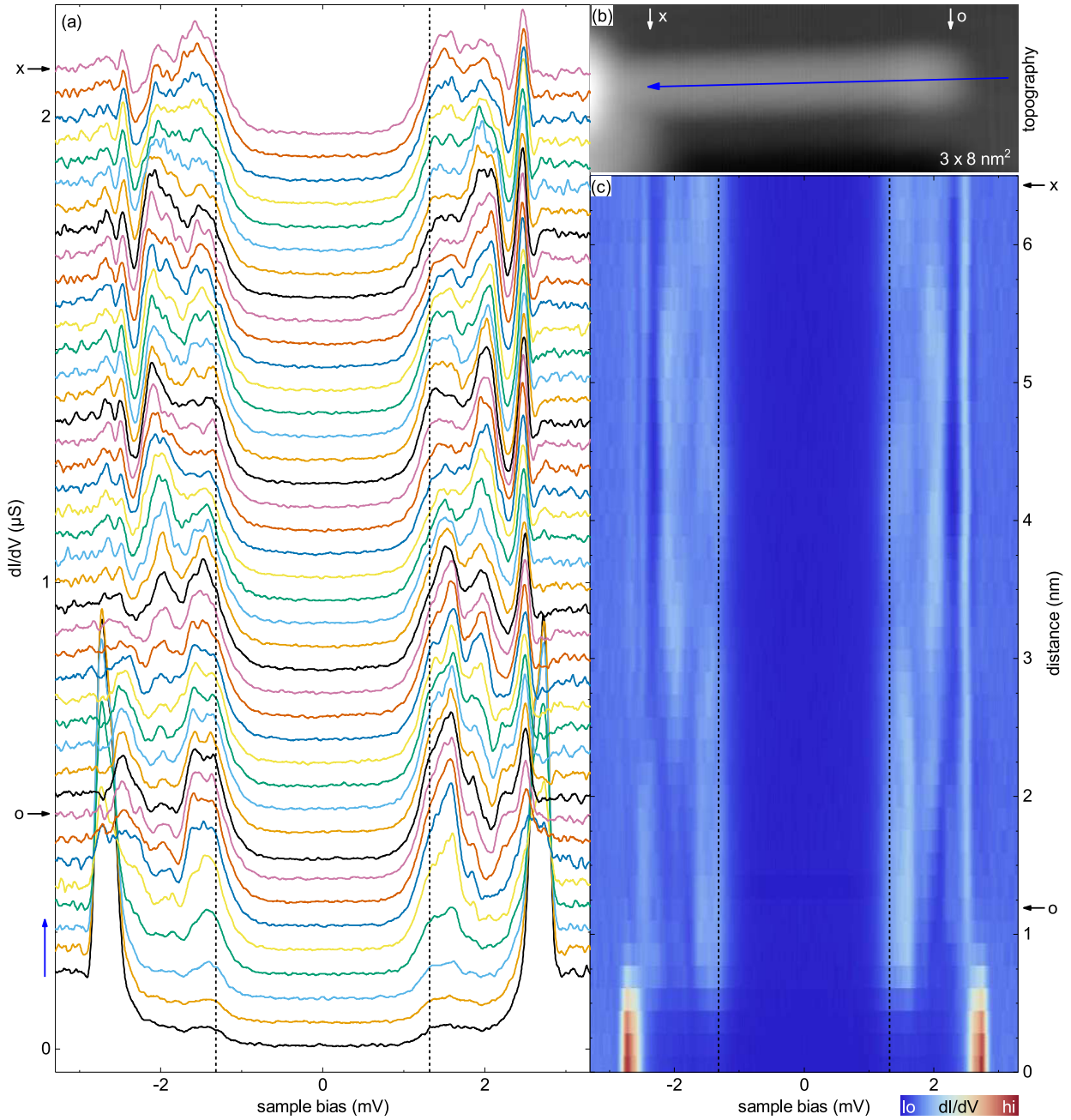

Figure S10: (a) Set of dI/dV spectra recorded at the Co chain on Pb(110) shown in (b) along the blue arrow. The chain is the same as the one in Fig. 4(c) of the main text. The chain length is $\simeq$ 6.1 nm. The spectra are offset for clarity by 50 nS. The lateral distance between the spectra is 167 pm. Tip gap: 1.32 meV. Setpoint: 4 mV, 500 pA. A false color plot of the spectral intensity of all spectra with respect to the lateral distance is shown in (c).

Tight binding band structure of a cobalt chain

Table S1: Slater-Koster tight-binding model parameters for Co (in eV). The spin-polarized orbital energies are denoted as ϵ. The hopping integral values V are calculated for the nearest-neighbor distance of bulk Co (hcp) with $a = 2.486$ Å.

Parameters	Spin up	Spin down
$\epsilon(d_{z^2})$	7.175	8.996
$\epsilon(d_{yz,xz})$	7.156	8.973
$\epsilon(d_{xy,x^2-y^2})$	7.197	9.011
$V(dd\sigma)$	-0.528	-0.599
$V(dd\pi)$	0.325	0.376
$V(dd\delta)$	-0.052	-0.060

In Fig. 5 of the main text, we show the band structure of a linear suspended cobalt chain, which is calculated using a tight binding model. The chain is aligned along the $\hat{\mathbf{z}}$ direction. The parameters are taken from Ref. 5, and are given in Tab. S1. The calculations first consider the d orbitals without spin-orbit coupling or superconductivity [Fig. 5(a) of the main text]. For each spin orientation, we obtain two doubly-degenerate bands from the $d_{\mathrm{xz,yz}}$ and $d_{\mathrm{xy,x^2-y^2}}$ orbitals, and a non-degenerate band from the $d_{\mathrm{z^2}}$ orbital. Notice that the band structure is very similar to the one of iron chains on Pb(110)[6].

A weak spin-orbit coupling lifts the degeneracy of the bands. We take this into account by adding the spin-orbit coupling Hamiltonian

$$H_{\mathrm{so}} = \lambda_{\mathrm{so}} \mathbf{L} \cdot \mathbf{s}, \tag{1}$$

where λ_{so} denotes the strength of the spin-orbit coupling, $\mathbf{L}$ is the orbital angular momentum of the electron and $\mathbf{s}$ is the spin angular momentum. The angle between the magnetization direction $\langle \mathbf{s} \rangle$ and $\hat{\mathbf{z}}$ is denoted as θ. The band structure with spin-orbit coupling for $\theta = \pi/2$ is shown in Fig. 5(b) of the main text. We use $\lambda_{\mathrm{so}} = 0.2$ eV, which is the same as the value for Fe in Ref. 7. If the magnetization is not perpendicular to the chain direction, the bands are further split. For $\theta = 2\pi/5$ and $\lambda_{\mathrm{so}} = 0.2$ eV, the band structure is shown in Fig. 5(c) of the main text.

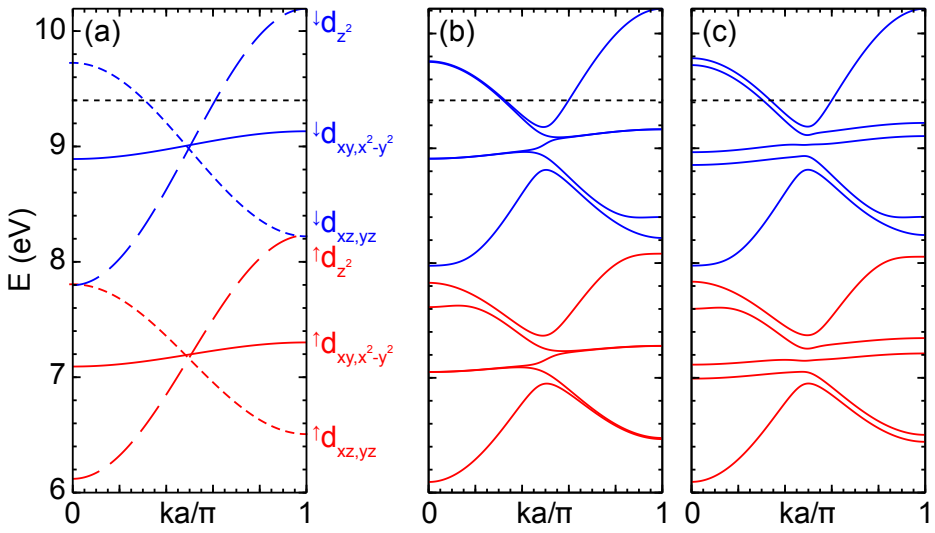

Figure S11: Tight-binding band structure of a linear suspended Co chain with interatomic distance $a = 2.486$ Å neglecting (a), or including (b,c) spin-orbit coupling, respectively. Spin-orbit coupling parameter: $\lambda_{so} = 0.2$ eV. The angle between the magnetization and the chain direction is $\pi/2$ (b) and $2\pi/5$ (c), respectively. The splitting between the minority (*blue*) and majority (*red*) bands is due to the exchange interaction. The horizontal black lines indicate a possible value of the chemical potential when considering a scenario with nine d electrons. This would predict three Fermi points and robust topological superconductivity.

Discussion of the band filling of cobalt chains on Pb(110)

The Fermi energy is a crucial property of the system, as it determines the number Fermi points within the band structure. Here we discuss two scenarios for a 1D Co chain, which result in different positions of the Fermi level.

In the main text, we discussed a scenario which is deduced from the single-atom limit. When a single Co atom is deposited onto a Pb surface, electrons can be transferred into the bulk Pb, and the Co atom becomes positively charged, presumably between Co^{2+} and Co^{3+}, the most common oxidation states of cobalt. This empties the s levels and partially the d levels. Thus, the number of valence (d) electrons per Co is between 6 and 7. We consider this a likely scenario and, hence, use it for the determination of the chemical potential in Figs. 5(b) and (c) of the main text.

A second scenario (see also Refs.[6,7]) is sketched for a Co chain in Fig. S11. Here, nine valence electrons per Co atom are assumed, which corresponds to the number of valence

electrons of a neutral Co atom. All nine electrons per atom presumably fill the d bands, because the s-derived bands lie higher in energy for the 1D chains. In this scenario, the Co chains always have three Fermi points in the band structure [Fig. S11(c)], and would be expected to exhibit robust topological superconductivity.

References

(1) Wiesendanger, R. *Rev. Mod. Phys.* **2009**, *81*, 1495.

(2) Pietzsch, O.; Kubetzka, A.; Bode, M.; Wiesendanger, R. *Phys. Rev. Lett.* **2004**, *92*, 057202.

(3) Ruby, M.; Heinrich, B. W.; Pascual, J. I.; Franke, K. J. *Phys. Rev. Lett.* **2015**, *114*, 157001.

(4) Ruby, M.; Pientka, F.; Peng, Y.; von Oppen, F.; Heinrich, B. W.; Franke, K. J. *Phys. Rev. Lett.* **2015**, *115*, 087001.

(5) Papaconstantopoulos, D. A. *Handbook of the band structure of elemental solids*. New York: Plenum Press **1986**.

(6) Nadj-Perge, S.; Drozdov, I. K.; Li, J.; Chen, H.; Jeon, S.; Seo, J.; MacDonald, A. H.; Bernevig, B. A.; Yazdani, A. *Science* **2014**, *346*, 602.

(7) Li, J.; Chen, H.; Drozdov, I. K.; Yazdani, A.; Bernevig, B. A.; MacDonald, A. H. *Phys. Rev. B* **2014**, *90*, 235433.